Electronic Supplementary Material (ESI) for Journal of Materials Chemistry A.

Support Information

Balancing Crystallization Rate in Mixed Sn-Pb Perovskite Film for Efficient and Stable Solar Cells Over 20% Efficiency

*Zhanfei Zhang, Jianghu Liang, Yiting Zheng, Xueyun Wu, Jianli Wang, Ying Huang, Yajuan Yang, Zhuang Zhou, Luyao Wang, Lingti Kong, Kolan Madhav Reddy, Chaochao Qin, Chun-Chao Chen**

Experimental

Materials

Lead(II) iodide (PbI_2, > 99.99%), methylammonium iodide (MAI, > 99.5%), formamidine iodide (FAI, >99.5%), bathocuproine (BCP), [6,6]-Phenyl-C61-butyric acid methyl ester (PCBM) were purchased from Xi'an Polymer Light Technology Crop. Tin(II) iodide (SnI_2, 99.99%), Tin(II) fluoride (SnF_2, 99%), N,N-Dimethylformamide (DMF, 99.8%), Dimethyl sulfoxide (DMSO, 99.8%), isopropanol (IPA), chlorobenzene (CB) and toluene were obtained from Sigma-Aldrich. i-Pentylammonium tetrafluoroborate ($C_5H_{14}BF_4N$, $[PNA]BF_4$) was gained from Greatcell Solar Materials Pty Ltd. Poly(3,4-ethylenedioxythiophene)-poly(styrenesulfonate) (PEDOT:PSS, Clevios^{TM} PVP AI 4083) was purchased from Heraues company.

Solution preparation

A total of 1.5 M Sn-Pb mixed perovskite $FA_{0.7}MA_{0.3}Sn_{0.5}Pb_{0.5}I_3$ precursor solution was prepared by dissolving 0.181 g of FAI, 0.072 g of MAI, 0.346 g of PbI_2, 0.279 g of SnI_2, and 0.012 g of SnF_2 in a mixed solvent of DMSO and DMF with a volume ratio of 1:3. The perovskite solution was filtered with polytetrafluoroethylene (PTFE) filters (0.22 μm) before use. The $[PNA]BF_4$ solution was prepared with a concentration of 0.2, 0.5, 0.8, and 1.0 mg/mL by dissolving in IPA. A total of 20 mg mL^{-1} PCBM in CB and 5 mg mL^{-1} BCP in IPA were prepared as electron transport material and hole barrier layer of the device respectively.

Device fabrication

The glass/ITO substrates (2.0*2.0 cm^2) were sequentially washed with deionized water, absolute ethanol, acetone and isopropanol in ultrasonic bath for 20 min. Then, the ITO substrates were further cleaned via UV-Ozone treatment for 15 min. After cooling down to room temperature, PEDOT:PSS solution was spin-coated on ITO substrates at 4000 rpm for 30 s and annealed at 150 °C for 10 min in ambient air. Then, the PEDOT:PSS-coated substrates were transferred into a nitrogen-filled glovebox, the $[PNA]BF_4$ solution with different concentration was spin-coated at 1,000 rpm for 30 s and thermal-annealed at 100 °C for 10 min. Then the $FA_{0.7}MA_{0.3}Sn_{0.5}Pb_{0.5}I_3$ perovskite films were deposited by spin-coating $FA_{0.7}MA_{0.3}Sn_{0.5}Pb_{0.5}I_3$ precursor solution onto PEDOT:PSS or $[PNA]BF_4$ film at 5,000 rpm for 60 s. Toluene was dropped onto the spinning substrate during the spin-coating. Then, perovskite films were annealed at 100 °C for 10 min. After that, the PCBM was spin-coated at 2000 rpm for 30 s and the BCP was deposited by spin-coating at 5000 rpm for 30 s. Finally, Ag (100 nm) was deposited as back electrode through a shallow mask by thermal evaporation under 9×10^{-5} Pa. The effective area of the electrode was 0.1 cm^2. All device measurements were unencapsulated and performed in ambient air with relative humidity of 30±5% at room temperature.

Characterization

The J-V characteristics of the as-prepared devices were tracked by a Keithley 2400 source measurement under a simulated AM 1.5G spectrum at 100 mW/cm^2 (Abet Technologies Sun 2000 solar simulator, calibrated with a standard VLSI Si reference solar cell (SRC-1000-TC-K-QZ), including reverse scanning ranges from

1.0 V to -0.2 V with an interval of 50 mV/s and forward scanning ranges from -0.2 V to 1.0 V with the same steps. The external quantum efficiency (EQE) spectra was recorded by the QTEST HIFINITY 5 EQE system (the light intensity was calibrated with Si detectors) in ambient air. Filed emission scanning electron microscopy (FESEM) images were acquired on JSM-7800F FE-SEM. Atom force microscopy (AFM) images were observed on the Bruke Bio-FastScan AFM using taping mode. Contact angle with water droplet was carried on the KRUSS GmbH DSA 100 contact angle measuring device. Steady state photoluminescence (PL) and time-resolved photoluminescence (TRPL) were conducted by FLS 1000 photoluminescence spectrometer by light incident from the perovskite film side and the excitation wavelength was 405 nm. Uv-vis absorption spectra and transmittance spectra was recorded by Lambda 35 Uv-vis spectrometer. X-ray photoelectron spectra (XPS) analysis were carried out using an Thermo Scientific K-Alpha X-ray photoelectron spectrometer and calibrated with C1s binding energy and curve fitting was performed using the Thermo Avantage software. Ultraviolet photoelectron spectroscopy (UPS) was measured by AXIS Ultra DLD machine. Electrochemical impedance spectroscopy (EIS) spectra was observed on a Chenhua CHI660E electrochemical workstation under dark conditions. FTIR spectra was recorded using a Thermo-Nicolet iS5 instrument. ToF-SIMS spectra was carried out using a GAIA3 GMU model 2016 scanning electron microscope.

Surface Residual Stress (Or Strain) Measurements

X-ray diffraction (XRD) patterns were detected with a Bruker D8 Advance X-

ray diffractometer under Cu K_α radiation and 4-50° scan range with a step size of 0.02 °/s. Diffraction patterns were collected as a function of θ angle of the thin film, using two different orthogonal orientations (Φ=0 and 90°) for confirming the isotropic nature of the residue stresses. The d spacings (110) for the well-defined XRD peaks at the highest 2θ angle (~14.2°) were used to generate the $\sin^2\psi$ plots. (110) interplanar spacing (d_{110}) is plotted as a function of $\sin^2\psi$ for $FA_{0.7}MA_{0.3}Pb_{0.5}Sn_{0.5}I_3$ perovskite film based on different concentration of $[PNA]BF_4$ ionic salt layers. The biaxial residual stress (σ_R) can be estimated from the $\sin^2\psi$ data using the following relation[1]:

$$\sigma_R = \left(\frac{E_{(110)}}{1+\nu}\right)\left(\frac{m}{d_n}\right)$$

Where m is the slope of the linear fit to the data, d_n is the d110 spacing at $\sin^2\psi$=0 (y intercept), $E_{(110)}$ is Young's modulus in the (110) direction, and v is the Poisson ratio. The $E_{(110)}$ of $FA_{0.7}MA_{0.3}Pb_{0.5}Sn_{0.5}I_3$ perovskite is estimated as 15 Gpa[2,3]. The typical v value of 0.3 is assumed[4].

Femtosecond Transient Absorption (fs-TA) measurements

Femtosecond Transient Absorption (fs-TA) measurements were performed on a Helios pump-probe system (Ultrafast Systems LLC) combined with an amplified femtosecond laser system (Coherent). Optical parametric amplifier (TOPAS-800-fs) provided a 500 nm pump pulse (~ 0.2 uJ $pulse^{-1}$ at the sample), which was excited by a Ti: sapphire regenerative amplifier (Legend Elite-1K-HE; 800 nm), 35 fs, 7 mJ $pulse^{-1}$, 1 kHz) and seeded with a mode-locked Ti: sapphire laser system (Micra 5) and an Nd: YLF laser (EvolutIon 30) pumped. Focusing the 800 nm beams (split from the regenerative amplifier with a tiny portion, ~400 nJ $pulse^{-1}$) onto a sapphire plate

produced the white-light continuum (WLC) probe pulses (820-1600 nm). The pulse-to-pulse fluctuation of the WLC is corrected by a reference beam split from WLC. A motorized optical delay line was used to change the time delays (0-8 ns) between the pump and probe pulses. The instrument response function (IRF) was determined to be ~100 fs by a routine cross-correlation procedure. The instrument response function (IRF) was determined to be ~100 fs by a routine cross-correlation procedure. A mechanical chopper operated at a frequency of 500 Hz used to modulate the pump pulses such that the fs-TA spectra with and without the pump pulses can be recorded alternately. The temporal and spectral profiles (chirp-corrected) of the pump-induced differential transmission of the WLC probe light (i.e., absorbance change) were visualized by an optical fiber-coupled multichannel spectrometer (with a CMOS sensor) and further processed by the Surface Xplorer software. The sample is measured by pump and probe polarizations oriented at the magic angle. According to the signal amplitude of femtosecond visible and near-infrared TA measurements, at least 5 scans were acquired and averaged to obtain a real data and the high signal-to-noise ratio (SNR) necessary for global analysis.

Density functional theory (DFT) calculations

We performed density functional theory (DFT) based first-principle calculation: We implemented Vienna Ab initio Simulation Package (VASP) code by using the projector-augmented wave (PAW) method. We adopted Perdew-Burke-Ernzerh (PBE) exchange correlation functional within the generalized gradient approximation (GGA). DFT-D3 method of Grimme is also applied to correct van der Waals (vdW)

interaction. The electron wave function basis set was expanded up to a cutoff energy of 500 eV. A 4×4×1 Monkhorst. Pack (MP) k mesh with a gamma k-point were adopted. For $MAPb_{0.5}Sn_{0.5}I_3$ (001)/$[PNA]BF_4$ absorption, a 15 Å vacuum layer is adopted to avoid the interaction between neighboring slabs. The convergence standard is set at 0.02 eV $Å^{-1}$ for total force of each atom, and the convergence threshold of energy for each atom is less than 1×10^{-5} eV. The dipole correction was calculated parallel to the z direction, and the potential correction mode (the LDIPOL tag) was also switched on in order to counterbalance the local potential and the force errors introduced by the periodic boundary conditions.

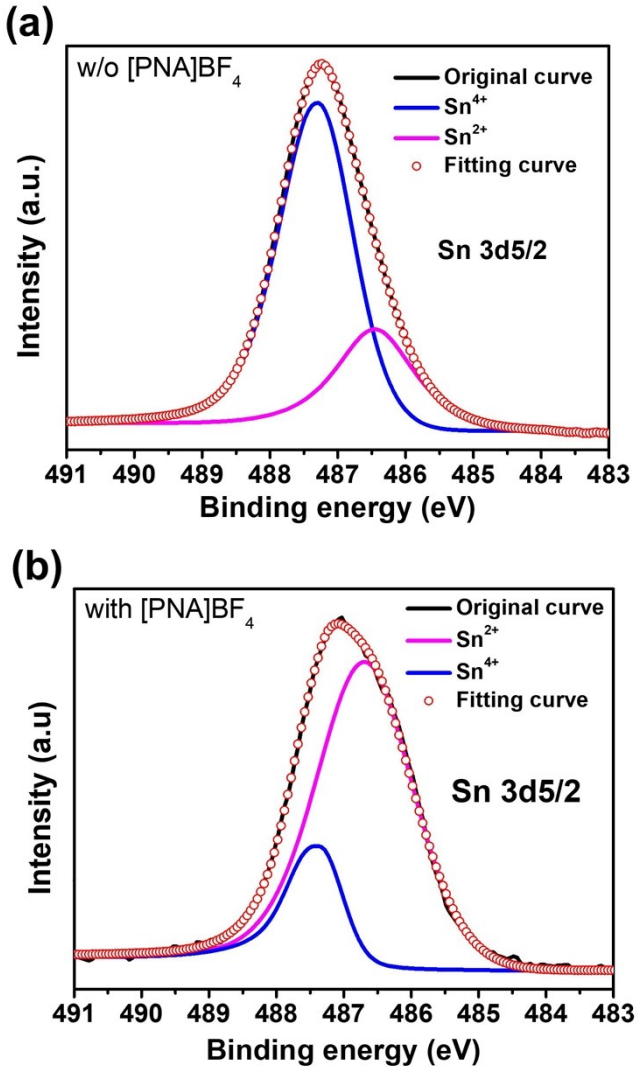

Figure S1 XPS spectra of Sn 3d for (a)pristine perovskite film and (b) perovskite film doped with [PNA]BF_4 ionic salts.

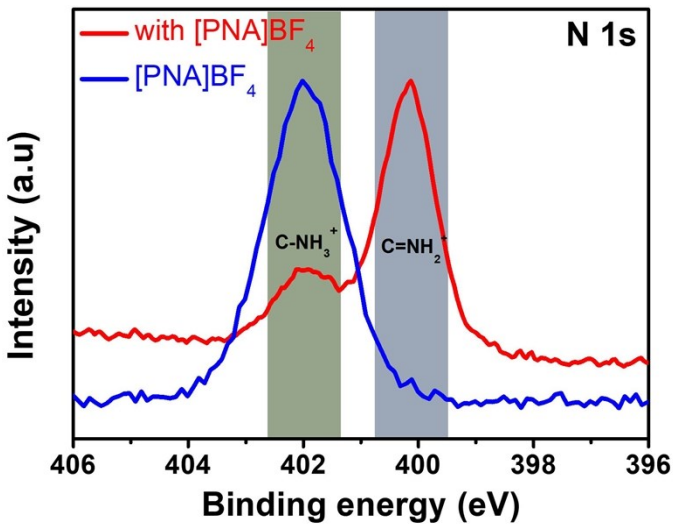

Figure S2 XPS spectra of N 1s for perovskite doped with $[PNA]BF_4$ and pristine $[PNA]BF_4$ ionic salts.

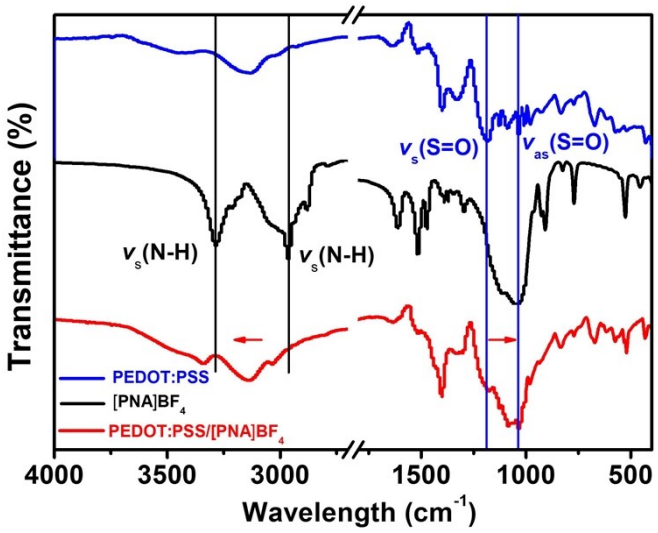

Figure S3 FTIR spectra of the PEDOT:PSS, $[PNA]BF_4$ and PEDOT:PSS/$[PNA]BF_4$ complex powder.

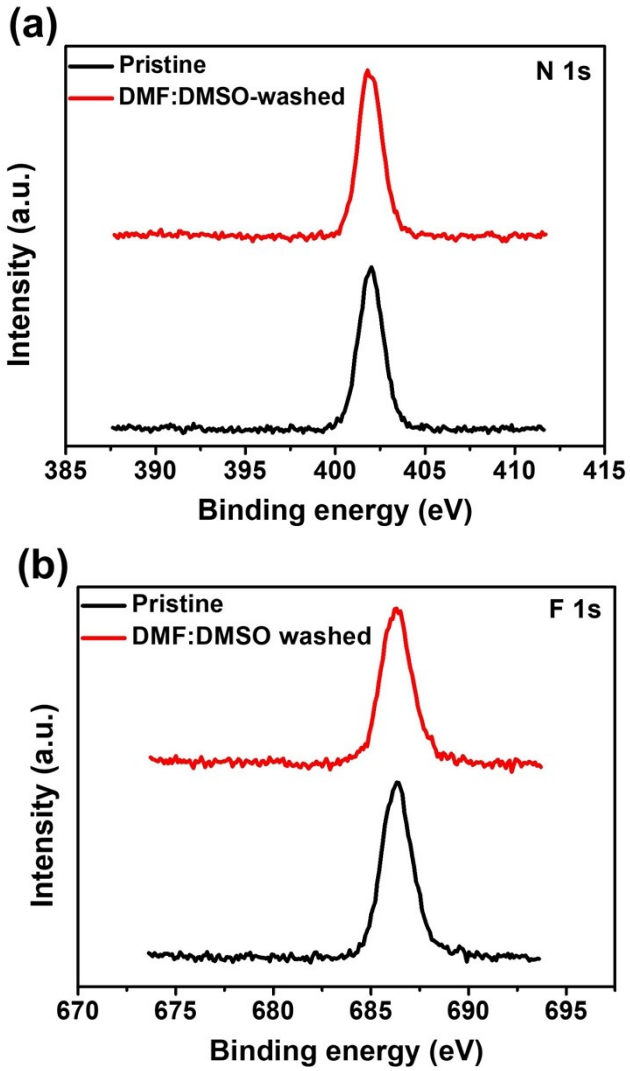

Figure S4 XPS spectra of the pristine [PNA]BF_4 film before and after washing with DMF:DMSO solvent.

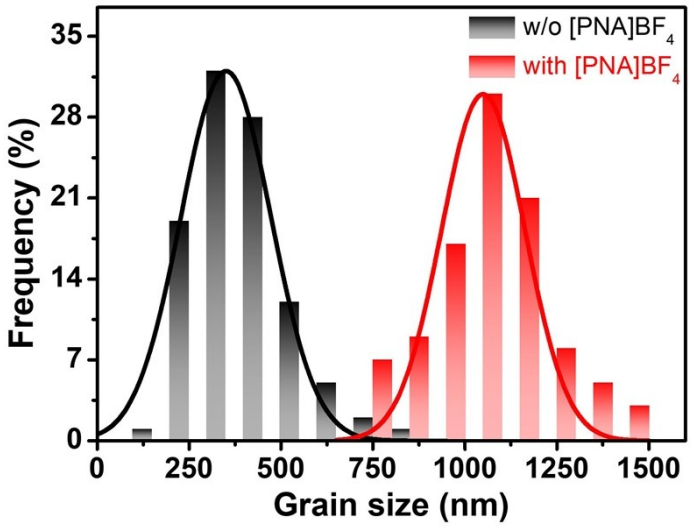

Figure S5 comparison of grain size distribution for perovskite film grown on PEDOT:PSS and [PNA]BF_4 ionic salt layer.

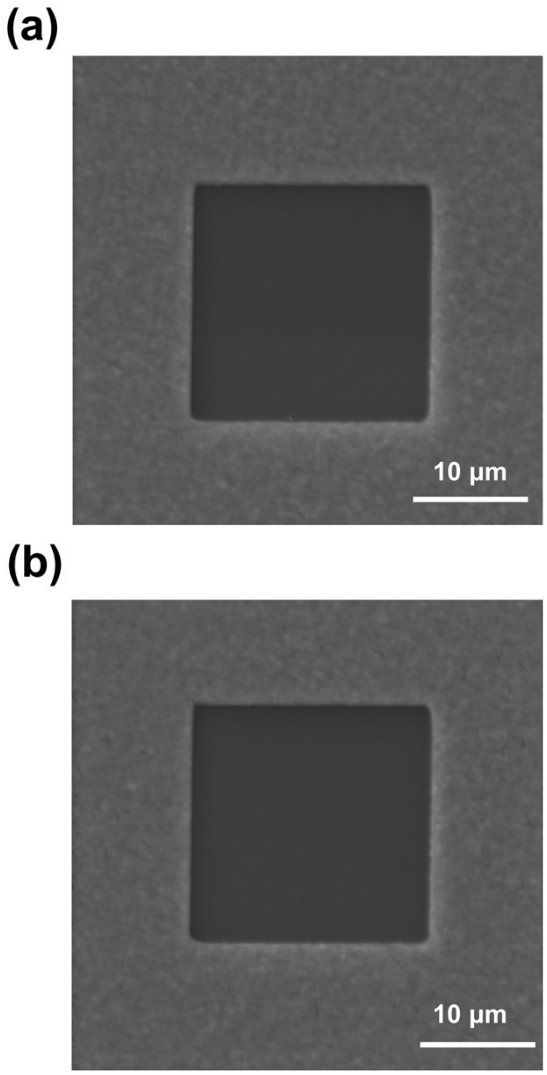

Figure S6 The top-view SEM images of final perovskite films after FIB etching during ToF-SIMS tests: (a) pristine perovskite film grown on PEDOT:PSS substrate; (b) perovskite film grown on [PNA]BF_4 doped PEDOT:PSS substrates.

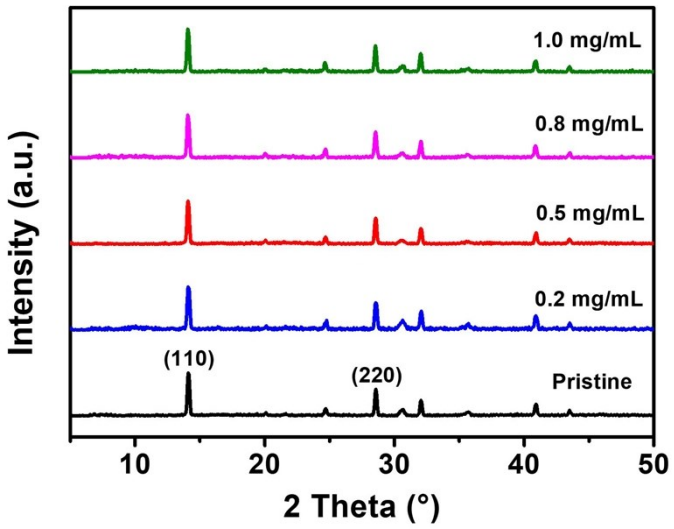

Figure S7 XRD spectra of perovskite films based on PEDOT:PSS and different concentration [PNA]BF_4 ionic salt layer.

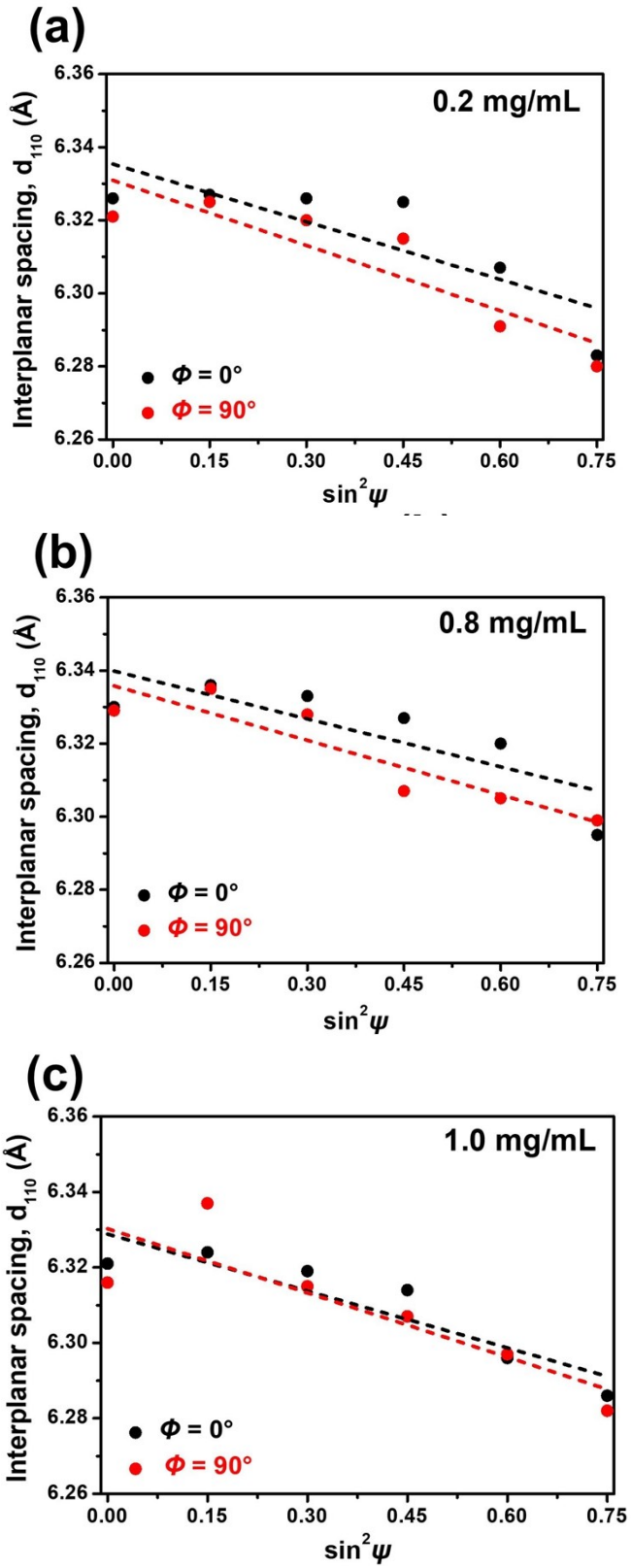

Figure S8 XRD d_{110} versus $\sin^2\Psi$ plots for perovskite film grown on different concentration of $[PNA]BF_4$ ionic salt layers: (a) 0.2 mg/mL; (b) 0.8 mg/mL; (c) 1.0 mg/mL.

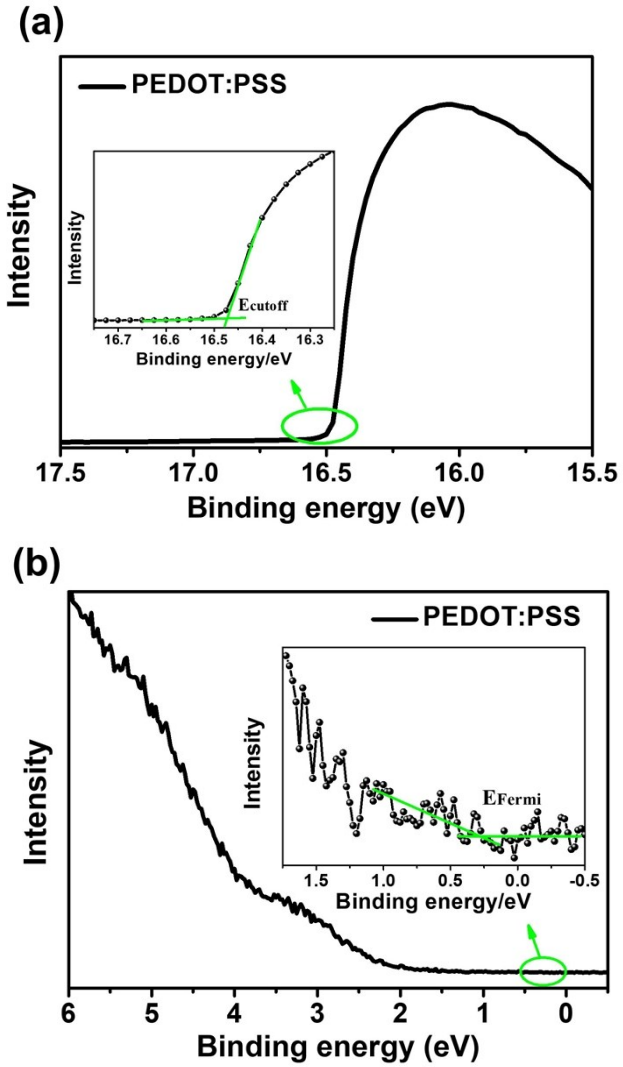

Figure S9 The UPS spectrum of pristine PEDOT:PSS film.

The work function (W_F) can be obtained from the equation as follows: $W_F = h\nu - E_{cutoff} = 21.22 - 16.47 = 4.75$ eV. The HOMO level can be obtained from the equation as follow: $HOMO = -W_F - E_{Fermi} = -4.75 - 0.27 = -5.02$ eV.

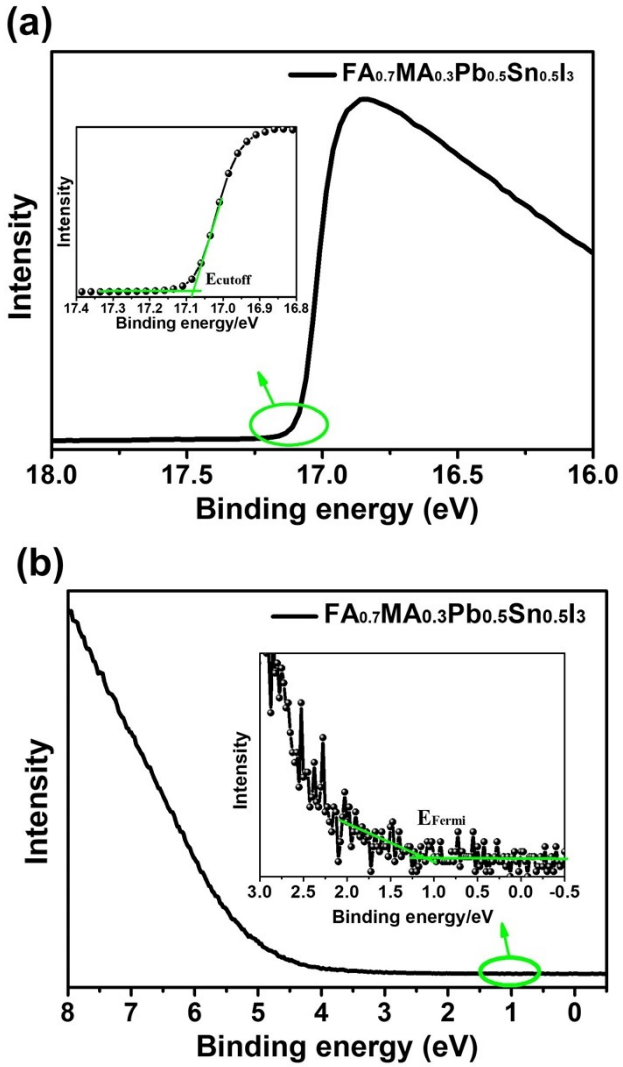

Figure S10 The UPS spectrum of $FA_{0.7}MA_{0.3}Pb_{0.5}Sn_{0.5}I_3$ perovskite film.

The work function (W_F) can be obtained from the equation as follows: $W_F = h\nu - E_{cutoff} = 21.22 - 17.08 = 4.14$ eV. The E_v can be obtained from the equation as follow: $E_v = -W_F - E_{Fermi} = -4.14 - 1.10 = -5.24$ eV. The E_c can be obtained from the equation as follow: $E_c = E_v + E_g = -5.24 + 1.24 = -4.00$ eV.

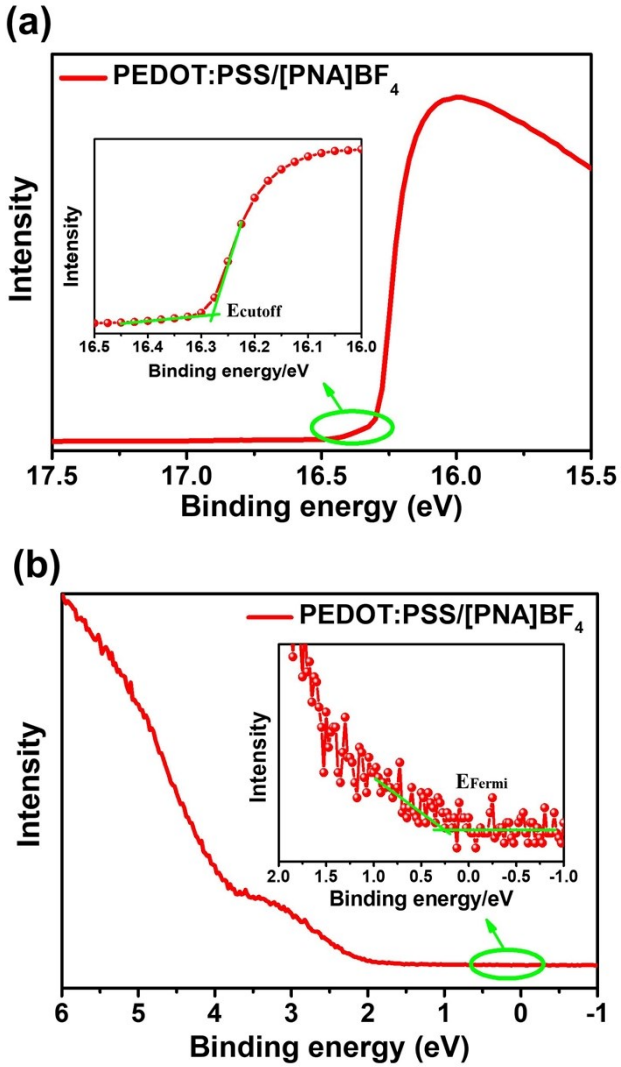

Figure S11 The UPS spectrum of $[PNA]BF_4$ modified PEDOT:PSS.

The work function (W_F) can be obtained from the equation as follows: $W_F = h\nu - E_{cutoff} = 21.22 - 16.27 = 4.95$ eV. The HOMO level can be obtained from the equation as follow: $HOMO = -W_F - E_{Fermi} = -4.95 - 0.27 = -5.22$ eV.

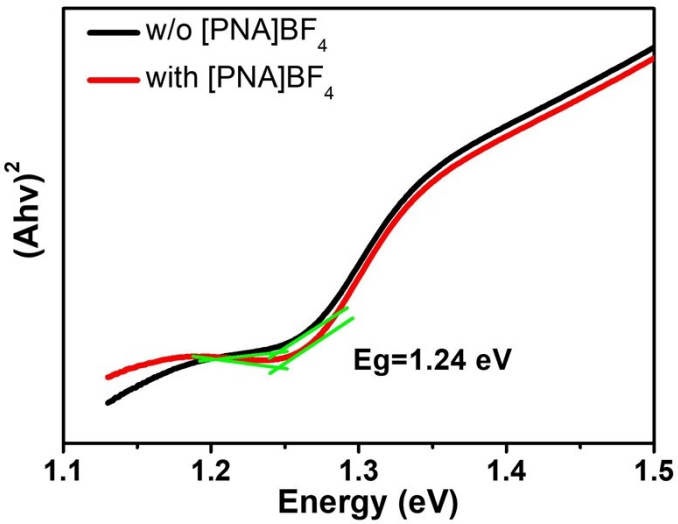

Figure S12 The relationship of $(Ahv)^2$ *vs* energy for $FA_{0.7}MA_{0.3}Pb_{0.5}Sn_{0.5}I_3$ grown on pristine PEDOT:PSS or PEDOT:PSS modified by $[PNA]BF_4$ ionic salts. The bandgap (Eg) of $FA_{0.7}MA_{0.3}Pb_{0.5}Sn_{0.5}I_3$ can be determined via linear extrapolation of the leading edges of the $(Ahv)^2$ curve to the base lines, both film corresponding to an optical bandgap of ~1.24 eV.

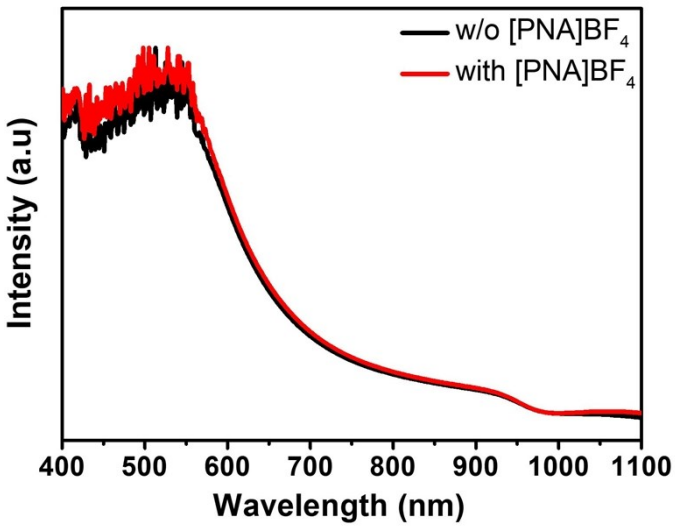

Figure S13 optical absorption spectra of $FA_{0.7}MA_{0.3}Sn_{0.5}Pb_{0.5}I_3$ film grown on pristine PEDOT:PSS and PEDOT:PSS modified by $[PNA]BF_4$ substrates.

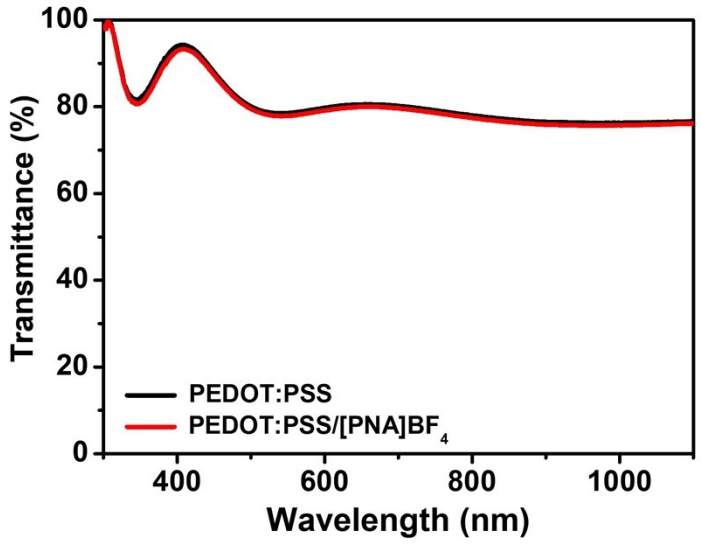

Figure S14 Transmission spectra of PEDOT:PSS and PEDOT:PSS coated with $[PNA]BF_4$.

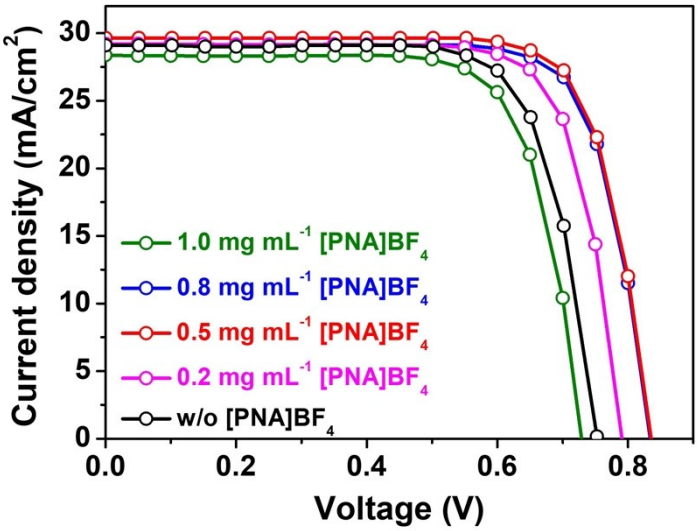

Figure S15 Current density-voltage (J-V) curves of PSCs treated by different concentration [PNA]BF_4 solutions

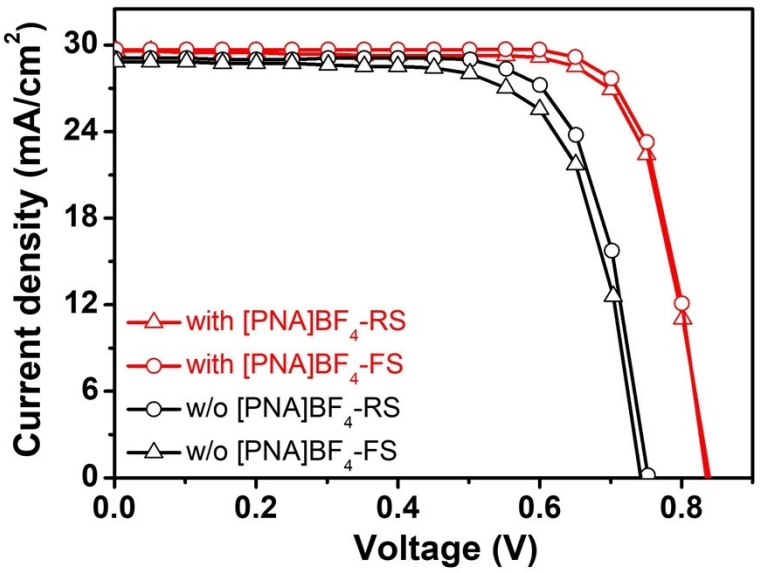

Figure S16 Current density-voltage (J-V) curves of the champion device with and without [PNA]BF_4 treatment in both forward and reverse scan direction.

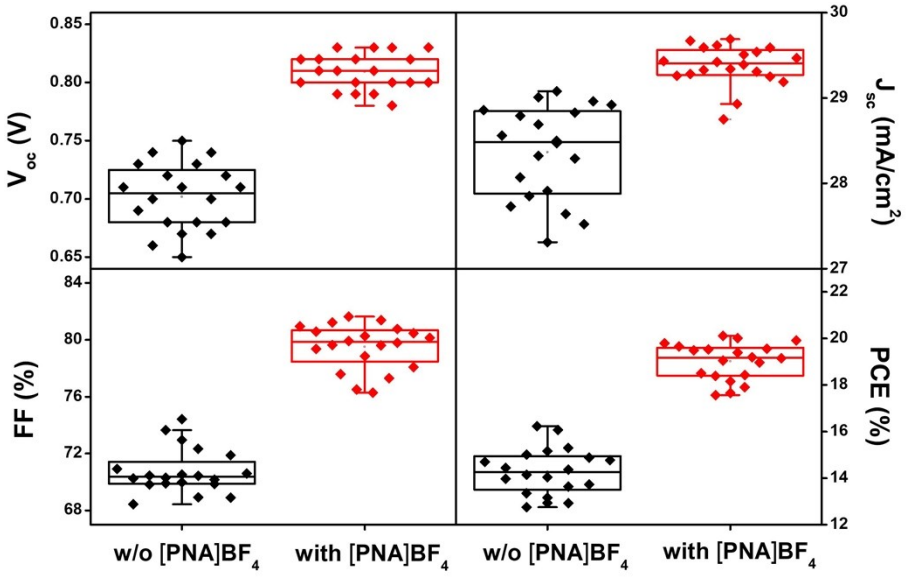

Figure S17 Statistics of V_{OC}, J_{SC}, FF, and PCE of 20 devices for control and $[PNA]BF_4$ treated perovskites.

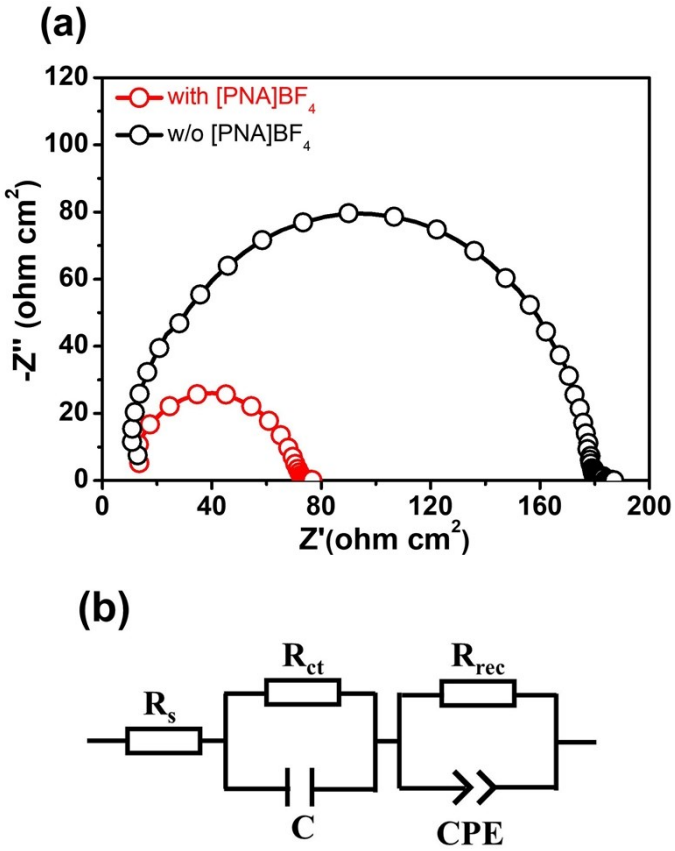

Figure S18 (a) Nyquist plots of PSCs with and without $[PNA]BF_4$ treatment; (b) Equivalent circuit of PSCs used for fitting impedance data.

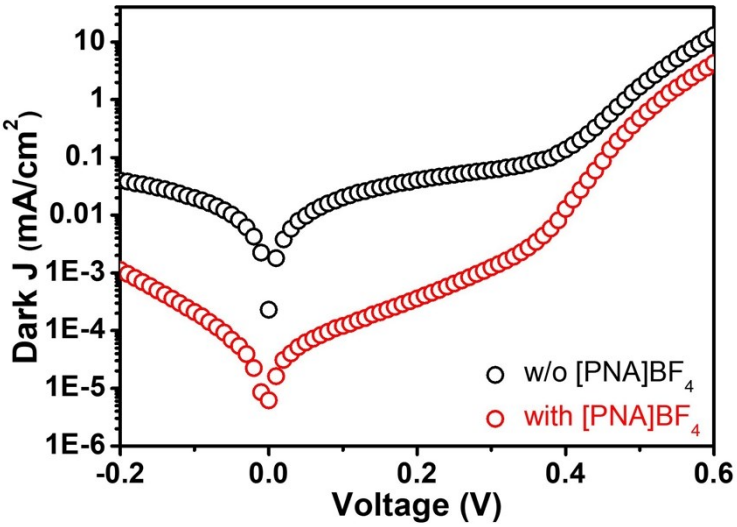

Figure S19 Dark J-V curves of PSCs with and without [PNA]BF_4 treatments.

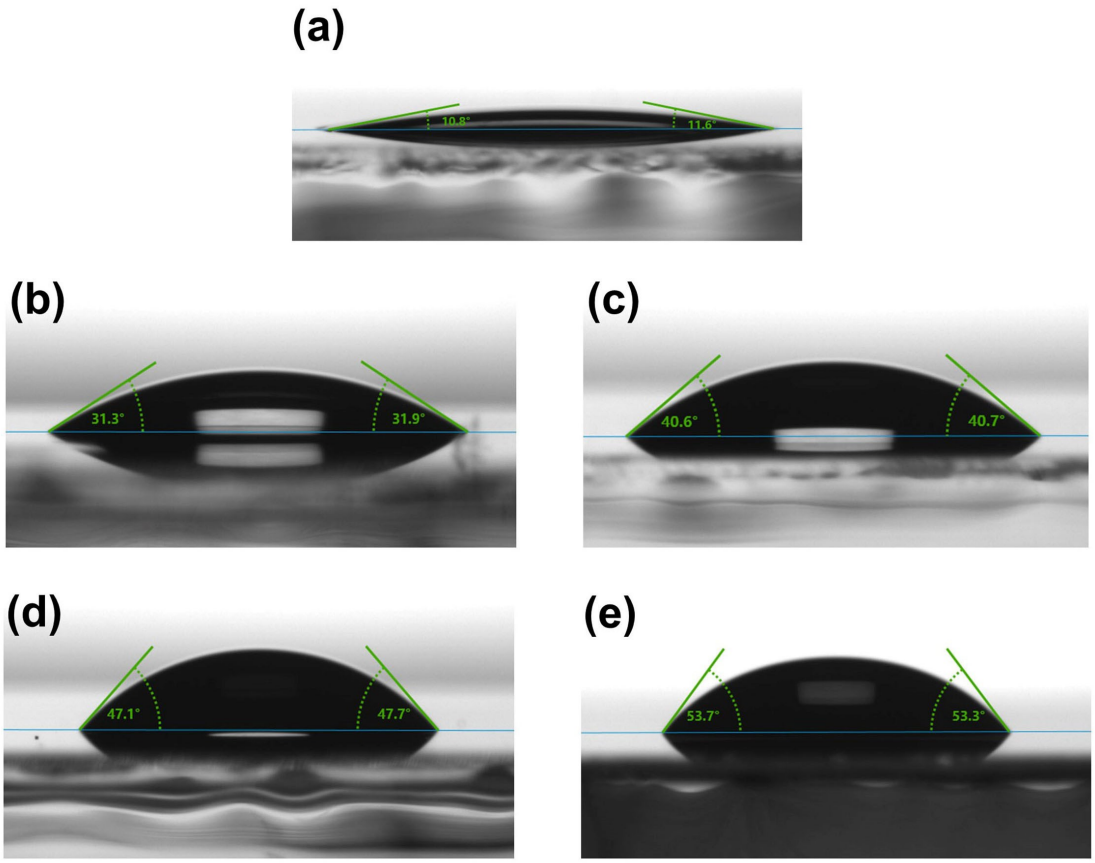

Figure S20 The contact angle images through water droplet on (a) pristine PEDOT:PSS surface and different concentration of [PNA]BF_4 ionic solution modified PEDOT:PSS: (b) 0.2 mg/mL, (c) 0.5 mg/mL, (d) 0.8 mg/mL and (e) 1.0 mg/mL.

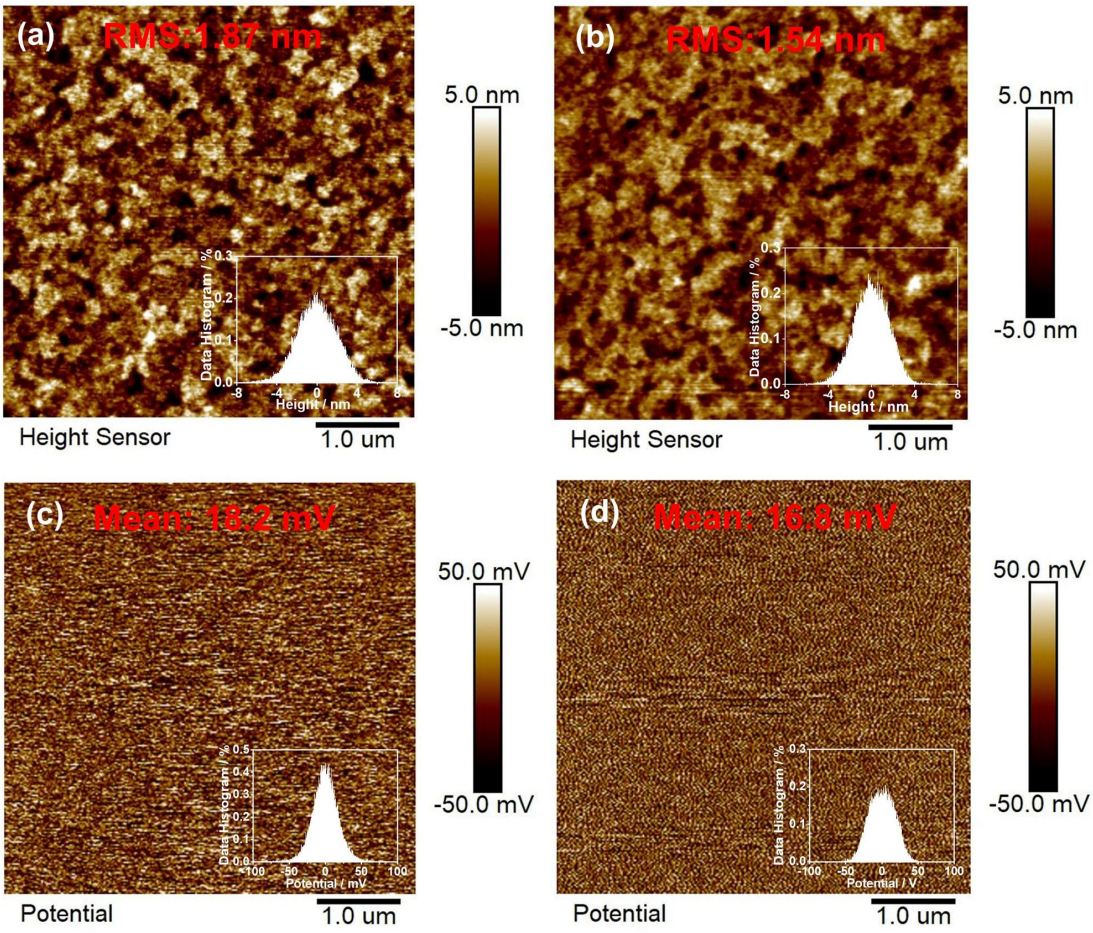

Figure S21 Top views AFM images of (a) PEDOT:PSS/ITO and (b) [PNA]BF_4/PEDOT:PSS/ITO; in-situ KPFM images of (c) and (d) corresponding to (a) and (b), respectively.

Table S1 The peak parameters and assignments of Sn 3d5/2 XPS for perovskite with and without doping of $[PNA]BF_4$ ionic salts.

Sample	Elemens	Binding energy/eV	FWHM[a)]/eV	Atomic ration/%	Affiliation
w/o $[PNA]BF_4$	Sn^{2+}	486.41	1.40	36.27	Sn^{2+}in $SnO_{1.39}$ [5]
	Sn^{4+}	487.29	1.27	63.73	Sn^{4+} in SnO_2 [6,7]
with $[PNA]BF_4$	Sn^{2+}	486.62	1.96	72.44	Sn^{2+} in SnO [8]
	Sn^{4+}	487.33	0.79	27.56	Sn^{4+} in SnO_2 [6,7]

a) FWHM: full width at half maximum.

Table S2 The peak parameters and assignments of B 1s, N 1s and Pb 4f XPS for pristine [PNA]BF_4, perovskite with and without doping of [PNA]BF_4 ionic salts.

Samples	Elements	Binding energy/eV	Affiliation
Pristine [PNA]BF_4	B 1s	194.71	B in NH_4BF_4 [9–11]
	N 1s	402.01	N 1s in NH_4Cl [12]
Perovskite doped with [PNA]BF_4	B 1s	187.23	B 1s in $NaBF_4$ [13]
	N 1s	402.08/400.13[a)]	N 1s in NH_4Cl, N 1s in CH_3CN [12,14]
	Pb 4f	137.73/142.58[b)]	[15,16]
Pristine perovskite	Pb 4f	138.03/142.83[b)]	[16,17]

a) (C-NH_3^+ / C=NH_2^+); b) (Pb $4f_{7/2}$ / Pb $4f_{5/2}$).

Table S3 The detailed photovoltaic parameters of champion PSCs with or without $[PNA]BF_4$.

Device	V_{oc}/V	J_{sc}/(mA/cm^2)	FF/%	PCE/%
1.0 mg mL^{-1}	0.72	28.36	73.31	14.95
0.8 mg mL^{-1}	0.83	29.12	78.69	19.02
0.5 mg mL^{-1}	0.83	29.62	81.62	20.11
0.2 mg mL^{-1}	0.79	29.21	78.46	18.11
Pristine	0.75	29.08	74.42	16.23

Table S4 The detailed photovoltaic parameters of champion PSCs with or without $[PNA]BF_4$.

Device	Scan	V_{oc}/V	J_{sc}/(mA/cm^2)	FF/%	PCE/%	Integrated J_{sc}/(mA/cm^2) from EQE
with $[PNA]BF_4$	Reverse	0.83	29.69	81.62	20.11	29.10
	Forward	0.83	29.59	80.56	19.78	
w/o $[PNA]BF_4$	Reverse	0.75	29.08	74.42	16.23	28.24
	Forward	0.74	28.83	70.51	15.04	

Table S5 lifetime and weight fractions fitted from TA decay curves.

Device	τ_1/ps	A_1/%	τ_2/ps	A_2/%	T_{ave}[a)]/ps
with $[PNA]BF_4$	1237.71	53.9	144.26	46.1	1138.59
w/o $[PNA]BF_4$	526.45	70.9	42.72	29.1	450.36

a) The τ_{ave} is calculated from the following equation: $\tau_{ave}=(A_1\tau_1^2+A_2\tau_2^2)/(A_1\tau_1+A_2\tau_2)$, representing the average lifetime of carries.

Table S6 lifetime and weight fractions fitted from TRPL decay curves.

Device	τ_1/ns	A_1/%	τ_2/ns	A_2/%	T_{ave}[a)]/ns
with $[PNA]BF_4$	0.85	88.7	10.69	11.3	6.91
w/o $[PNA]BF_4$	0.46	96.9	5.67	3.1	1.93

a) The τ_{ave} is calculated from the following equation: $\tau_{ave}=(A_1\tau_1^2+A_2\tau_2^2)/(A_1\tau_1+A_2\tau_2)$, representing the average lifetime of carries.

Table S7 The related parameters fitted from the equivalent circuit for EIS spectra measurement.

Device	R_s/Ω	R_{ct}/Ω	C/nF	R_{rec}/Ω	CPE/nF
with $[PNA]BF_4$	12.27	5.45	164.9	53.85	20.60
w/o $[PNA]BF_4$	55.01	169.30	14.7	6.57	118.50

Table S8 Performance comparison of reported highly efficient invert NBG (less than 1.3 eV) PSCs.

Composition	J_{sc}/(mA/cm^2)	V_{oc}/V	FF/%	PCE/%	References
$MAPb_{0.5}Sn_{0.5}I_3$	26.3	0.75	69	13.6	[18]
$MAPb_{0.5}Sn_{0.5}I_3$	25.5	0.84	67	14.4	[19]
$MAPb_{0.5}Sn_{0.5}I_3$	26.2	0.87	69	15.2	[20]
$FA_{0.75}Cs_{0.25}Pb_{0.5}Sn_{0.5}I_3$	26.7	0.74	71	14.1	[21]
$(FASnI_3)_{0.6}(MAPbI_3)_{0.4}$	26.9	0.80	71	15.1	[22]
$FA_{0.66}MA_{0.34}Pb_{0.5}Sn_{0.5}I_3$	27.8	0.78	73	15.9	[23]
$(FASnI_3)_{0.6}(MAPbI_3)_{0.4}$	28.7	0.85	71	17.5	[24]
$(FASnI_3)_{0.6}(MAPbI_3)_{0.4}$	27.6	0.84	73	17.8	[25]
$(FASnI_3)_{0.6}(MAPbI_3)_{0.4}$	29.0	0.84	74	18.1	[26]
$(FASnI_3)_{0.6}(MAPbI_3)_{0.4}$	27.3	0.83	80	18.2	[27]
$MA_{0.2}FA_{0.7}Cs_{0.1}Pb_{0.5}Sn_{0.5}I_3$	30.7	0.79	77.7	18.9	[28]
$FA_{0.5}MA_{0.5}Pb_{0.5}Sn_{0.5}I_3$	31.4	0.81	75.2	19.1	[29]
$FA_{0.6}MA_{0.4}Sn_{0.6}Pb_{0.4}I_3$	30.4	0.834	80.8	20.5	[30]
$FA_{0.7}MA_{0.3}Pb_{0.5}Sn_{0.5}I_3$	30.63	0.839	81.1	20.84	[31]
$FA_{0.7}MA_{0.3}Pb_{0.5}Sn_{0.5}I_3$	29.69	0.83	81.62	20.11	This work

References

1 M. Birkholz, *Thin Film Analysis by X-Ray Scattering*, 2006.

2 S. Sun, Y. Fang, G. Kieslich, T. J. White and A. K. Cheetham, *J. Mater. Chem. A*, 2015, **3**, 18450–18455.

3 N. Rolston, K. A. Bush, A. D. Printz, A. Gold-Parker, Y. Ding, M. F. Toney, M. D. McGehee and R. H. Dauskardt, *Adv. Energy Mater.*, 2018, **8**, 1802139.

4 J. Feng, *APL Mater.*, 2014, **2**, 081801.

5 W. Choi, H. Jung and S. Koh, *J. Vac. Sci. Technol. A Vacuum, Surfaces, Film.*, 1996, **14**, 359–366.

6 Ş. Süzer, T. Voscoboinikov, K. R. Hallam and G. C. Allen, *Fresenius. J. Anal. Chem.*, 1996, **355**, 654–656.

7 M. Di Giulio, A. Serra, A. Tepore, R. Rella, P. Siciliano and L. Mirenghi, *Mater. Sci. Forum*, 1996, **203**, 143–148.

8 P. A. Grutsch, M. V. Zeller and T. P. Fehlner, *Inorg. Chem.*, 1973, **12**, 1431–1433.

9 V. Y. Rosolovskii, V. I. Nefedov and S. M. Sinel'nikov, *Bull. Acad. Sci. USSR Div. Chem. Sci.*, 1973, **22**, 1407–1409.

10 B. R. Strohmeier, *Appl. Surf. Sci.*, 1989, **40**, 249–263.

11 M. Barber, J. A. Connor, M. F. Guest, I. H. Hillier, M. Schwarz and M. Stacey, *J. Chem. Soc. Faraday Trans. 2 Mol. Chem. Phys.*, 1973, **69**, 551–558.

12 M. Datta, H. J. Mathieu and D. Landolt, *Appl. Surf. Sci.*, 1984, **18**, 299–314.

13 D. N. Hendrickson, J. M. Hollander and W. L. Jolly, *Inorg. Chem.*, 1970, **9**, 612–615.

14 B. A. Sexton and N. R. Avery, *Surf. Sci.*, 1983, **129**, 21–36.

15 V. I. Nefedov, M. N. Firsov and I. S. Shaplygin, *J. Electron Spectros. Relat. Phenomena*, 1982, **26**, 65–78.

16 A. R. H. F. Ettema and C. Haas, *J. Phys. Condens. Matter*, 1993, **5**, 3817–3826.

17 D. G. Castner, K. Hinds and D. W. Grainger, *Langmuir*, 1996, **12**, 5083–5086.

18 Y. Li, W. Sun, W. Yan, S. Ye, H. Rao, H. Peng, Z. Zhao, Z. Bian, Z. Liu, H. Zhou and C. Huang, *Adv. Energy Mater.*, 2016, **6**, 1601353.

19 A. Rajagopal, Z. Yang, S. B. Jo, I. L. Braly, P.-W. Liang, H. W. Hillhouse and A. K.-Y. Jen, *Adv. Mater.*, 2017, **29**, 1702140.

20 A. Rajagopal, P. W. Liang, C. C. Chueh, Z. Yang and A. K. Y. Jen, *ACS Energy Lett.*, 2017, **2**, 2531–2539.

21 G. E. Eperon, S. D. Stranks, C. Menelaou, M. B. Johnston, L. M. Herz and H. J. Snaith, *Energy Environ. Sci.*, 2014, **7**, 982–988.

22 W. Liao, D. Zhao, Y. Yu, N. Shrestha, K. Ghimire, C. R. Grice, C. Wang, Y. Xiao, A. J. Cimaroli, R. J. Ellingson, N. J. Podraza, K. Zhu, R. G. Xiong and Y. Yan, *J. Am. Chem. Soc.*, 2016, **138**, 12360–12363.

23 J. Wang, K. Datta, J. Li, M. A. Verheijen, D. Zhang, M. M. Wienk and R. A. J. Janssen, *Adv. Energy Mater.*, 2020, **10**, 2000566.

24 D. Zhao, Y. Yu, C. Wang, W. Liao, N. Shrestha, C. R. Grice, A. J. Cimaroli, L. Guan, R. J. Ellingson, K. Zhu, X. Zhao, R. G. Xiong and Y. Yan, *Nat. Energy*, 2017, **2**, 17018.

25 G. Xu, P. Bi, S. Wang, R. Xue, J. Zhang, H. Chen, W. Chen, X. Hao, Y. Li and Y. Li, *Adv. Funct. Mater.*, 2018, **28**, 1804427.

26 D. Zhao, C. Chen, C. Wang, M. M. Junda, Z. Song, C. R. Grice, Y. Yu, C. Li, B. Subedi, N. J. Podraza, X. Zhao, G. Fang, R. G. Xiong, K. Zhu and Y. Yan, *Nat. Energy*, 2018, **3**, 1093–1100.

27 A. Goyal, S. McKechnie, D. Pashov, W. Tumas, M. Van Schilfgaarde and V. Stevanović, *Chem. Mater.*, 2018, **30**, 3920–3928.

28 M. Wei, K. Xiao, G. Walters, R. Lin, Y. Zhao, M. I. Saidaminov, P. Todorović, A. Johnston, Z. Huang, H. Chen, A. Li, J. Zhu, Z. Yang, Y. Wang, A. H. Proppe, S. O. Kelley, Y. Hou, O. Voznyy, H. Tan and E. H. Sargent, *Adv. Mater.*, 2020, **32**, 1907058.

29 H. Kim, J. W. Lee, G. R. Han, S. K. Kim and J. H. Oh, *Adv. Funct. Mater.*, 2021, **31**, 2008801.

30 J. Tong, Z. Song, D. H. Kim, X. Chen, C. Chen, A. F. Palmstrom, P. F. Ndione, M. O. Reese, S. P. Dunfield, O. G. Reid, J. Liu, F. Zhang, S. P. Harvey, Z. Li, S. T. Christensen, G. Teeter, D. Zhao, M. M. Al-Jassim, M. F. A. M. Van Hest, M. C. Beard, S. E. Shaheen, J. J. Berry, Y. Yan and K. Zhu, *Science (80-.).*, 2019, **364**, 475–479.

31 K. Xiao, R. Lin, Q. Han, Y. Hou, Z. Qin, H. T. Nguyen, J. Wen, M. Wei, V. Yeddu, M. I. Saidaminov, Y. Gao, X. Luo, Y. Wang, H. Gao, C. Zhang, J. Xu, J. Zhu, E. H. Sargent and H. Tan, *Nat. Energy*, 2020, **5**, 870–880.